Resonance Raman Spectroscopy of Iron(III) Tetrathiolate Complexes: Implications for the Conformation and Force Field of Rubredoxin

Roman S. Czernuszewicz,*,† LaTonya K. Kilpatrick,‡ Stephen A. Koch,§ and Thomas G. Spiro*,‡

Contribution from the Departments of Chemistry, University of Houston, Houston, Texas 77004, Princeton University, Princeton, New Jersey 08544, and State University of New York, Stony Brook, New York 11794

Received December 17, 1993®

Abstract: Vibrational spectra are analyzed for a series of iron(III) tetrathiolate complexes, including $[Fe(SMe)_4]^-$, $[Fe(SEt)_4]^-$, and $[Fe(S_2\text{-}o\text{-}xyl)_2]^-$ (SMe = methylthiolate, SEt = ethylthiolate, and S_2-*o*-xyl = *o*-xylene-α,α'-dithiolate), using resonance Raman (RR) and infrared spectra of isotopomers (^{54}Fe, ^{34}S, and ^2H). Assignments are made with the aid of normal coordinate analysis calculations, using a consistent force field for all three species. These results permit reanalysis and modeling of previously published RR spectra of oxidized rubredoxin in which Fe^{3+} is bound by four cysteinate side chains. The spectra of the analog complexes reveal (1) symmetry lowering from T_d, manifested in the splitting of the triply degenerate ν_3 Fe—S stretching mode, due to the S—C bonds being oriented out of the S—Fe—S planes; (2) further splitting, in the case of $[Fe(SMe)_4]^-$, due to inequivalence of the S—Fe—S angles; (3) elevation of the ν_1 Fe—S breathing frequency via interaction with methyl torsional modes in $[Fe(SEt)_4]^-$; and (4) mixing of Fe—S stretching and S—C—C bending modes due to the chelate ring constraints in $[Fe(S_2\text{-}o\text{-}xyl)_2]^-$. The rubredoxin RR bands and ^{54}Fe isotope shifts are modeled with the same force field, revealing a dominant influence of Fe—S/S—C—C mixing due to 180° FeS—CC dihedral angles for two of the cysteinate ligands. Proper calculation of the ν_1 frequency of rubredoxin requires a significant reduction of the Fe—S stretching force constant, relative to that of the analog complexes. This reduction is proposed to reflect the influence of H-bonding to the cysteinate S atoms in the protein.

Introduction

Iron–sulfur proteins, in which ferric or ferrous ions are bound in sulfur coordination environments,[1] are ubiquitous in biology. They mostly act as one-electron transfer agents in biological electron transport chains, but nonredox functions have been discovered for many Fe—S proteins. The simplest members of the class are the rubredoxins (Rd), which have a single Fe ion, tetrahedrally coordinated by four cysteine side chains.[2] Other members have two or more iron ions in a cluster, bridged by sulfide ions.

The Fe—S proteins are brown in color, due to visible absorption bands which are associated with S → Fe charge-transfer (CT) transitions.[3] Resonance Raman (RR) spectra[4] show selective enhancement of Fe—S vibrations, due to the extension of the Fe—S bonds in the CT excited states. The RR spectral patterns are characteristic of the different structural types, and they have been assigned and analyzed with the aid of isotopic substitution, model compound studies, and normal coordinate analysis.

Surprisingly, Rd spectra have been the least well understood, despite the simplicity of the $Fe(SR)_4$ structural motif. The initially reported spectrum,[5] one of the first RR spectra of a biological molecule, was interpreted as arising from a simple tetrahedral complex: a strong, polarized band at 314 cm^{-1}, assigned to the breathing mode, ν_1, a weaker depolarized band at 368 cm^{-1}, assigned to the triply degenerate stretch, ν_3, and weak bands at 150 and 126 cm^{-1}, assigned to the doubly and triply degenerate bending modes, ν_2 and ν_4. Indeed the spectrum appeared to be very similar to that of the isoelectronic complex $[FeCl_4]^-$.[6] Subsequent studies,[7,8] with better spectral quality and with isotope shift data, have uncovered considerable complexity, however. The principal issues are that (1) the ν_3 band actually consists of three widely spaced components, at 343, 363, and 376 cm^{-1}; (2) their $^{54/56}Fe$ isotope shifts indicate substantial mixing with other coordinates, not involving Fe motion; and (3) the ν_1 frequency is 16 cm^{-1} higher than that of the analog complex $[Fe(S_2\text{-}o\text{-}xyl)_2]^-$ (S_2-*o*-xyl = *o*-xylene-α,α'-dithiolate), despite essentially identical Fe—S bond distances.[9] In analyzing the analog complex spectra, Yachandra *et al.*[7] suggested that these deviations from the spectral pattern expected for an FeS_4 tetrahedron might result from differential mixing of the Fe—S stretching coordinates with S—C—C bending coordinates, which have similar natural frequencies. The phenomenon of Fe—S/S—C—C coordinate mixing has since been firmly established for other iron–sulfur

* Authors to whom correspondence should be addressed.
† University of Houston.
‡ Princeton University.
§ State University of New York.
® Abstract published in *Advance ACS Abstracts,* July 1, 1994.

(1) *Iron-Sulfur Proteins*; Spiro, T. G., Ed.; Wiley-Interscience: New York, 1982.

(2) (a) Watenpaugh, K. D.; Sieker, L. C.; Jensen, L. H. *J. Mol. Biol.* **1979**, *131*, 509–522. (b) Watenpaugh, K. D.; Sieker, L. C.; Jensen, L. H. *J. Mol. Biol.* **1980**, *138*, 615. (c) Sieker, L. C.; Stenkamp; R. E.; Jensen, L. H.; Prickril, B.; LeGall, J. *FEBS Lett.* **1986**, *208*, 73–76. (d) Frey, M.; Sieker, L. C.; Payan, F.; Haser, R.; Bruschi, M.; Pepe, G.; LeGall, J. *J. Mol. Biol.* **1987**, *197*, 525–541. (e) Adman, E.; Sieker, L. C.; Jensen, L. H. *J. Mol. Biol.* **1991**, *217*, 337–351.

(3) Eaton, W. A.; Lovenberg, W. In *Iron-Sulfur Proteins*; Lovenberg, W., Ed.; Academic Press: New York, 1973; Vol. 2, Chapter 3.

(4) Spiro, T. G.; Czernuszewicz, R. S.; Han, S. In *Biological Applications of Raman Spectroscopy*; Spiro, T. G., Ed.; John Wiley & Sons, Inc.: New York, 1987; Vol. 3, pp 523–553.

(5) (a) Long, T. V.; Loehr, T. M. *J. Am. Chem. Soc.* **1970**, *92*, 6384–6386. (b) Long, T. V.; Loehr, T. M.; Allkins, J. R.; Lovenberg, W. J. *J. Am. Chem. Soc.* **1971**, *93*, 1809–1811.

(6) Nakamoto, K. *Infrared and Raman Spectra of Inorganic and Coordination Compounds*; Wiley-Interscience: New York, 1986.

(7) Yachandra, V. K.; Hare, J.; Moura, I.; Spiro, T. G. *J. Am. Chem. Soc.* **1983**, *105*, 6455–6462.

(8) Czernuszewicz, R. S.; LeGall, J.; Moura, I.; Spiro, T. G. *Inorg. Chem.* **1986**, *25*, 696–700.

(9) (a) Lane, R. W.; Ibers, J. A.; Frankel, R. B.; Holm, R. H. *Proc. Natl. Acad. Sci. U.S.A.* **1975**, *72*, 2868–2872. (b) Lane, R. W.; Ibers, J. A.; Frankel, R. B.; Papaefthymiou, G. C.; Holm, R. C. *J. Am. Chem. Soc.* **1977**, *99*, 84–98.

0002-7863/94/1516-7134$04.50/0

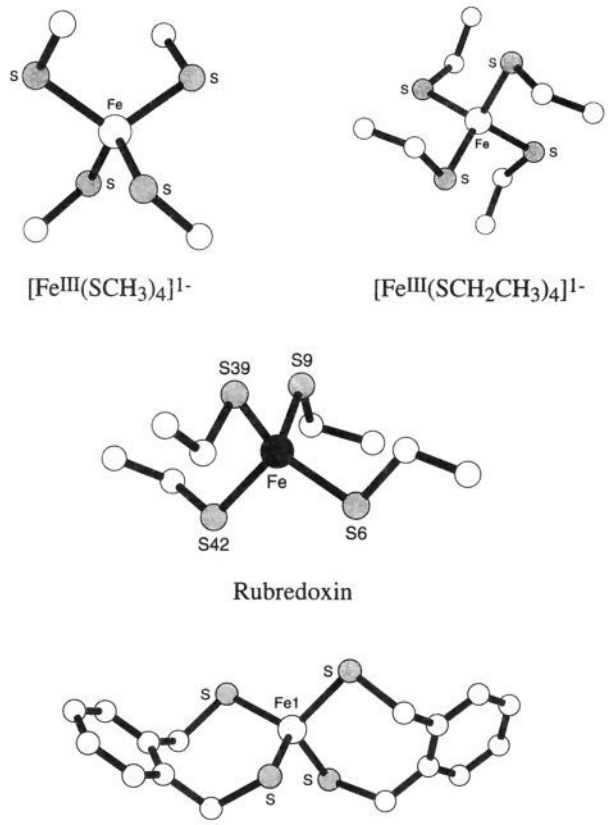

Figure 1. Structural diagrams for Rd and its analogs.

structural types[10,11] and helps to account for the variability in spectral pattern of the Fe—S(Cys) modes. Recently, Saito *et al.*[12] reported a calculation of all the modes of the non-hydrogen atoms in Rd and found extensive mixing of Fe—S stretching with numerous bending coordinates, distributed over some 15 residues of the protein. The accuracy of this very complicated mode description is difficult to assess, however.

In the present study we aim to describe the main features of the Rd RR spectrum by analyzing the vibrational modes of a series of small molecule analogs, which exemplify different kinds of mode mixing.

Materials and Methods

Preparation of Analog Complexes. All synthetic steps were performed under a dry dinitrogen atmosphere using Schlenk techniques or in an O_2-free drybox. The solvents were freshly distilled and degassed with four freeze–pump–thaw cycles.

$(Et_4N)[Fe(SCH_3)_4]$ and $(Pr_4N)[Fe(SC_2H_5)_4]$ were prepared via ligand exchange reactions of the respective alkylthiols with the Fe(III) tetraphenolate complex, as described in ref 13. Methane and ethane thiols were purchased from Aldrich Chemical Co. (Milwaukee, WI) and were used without further purification. The deuterated isotopomers were prepared by the same method, utilizing the CD_3SH and C_2D_5SH thiols (98% enriched, ICON Services, Summit, NJ). The methanetetrathiolate complex with ^{54}Fe was obtained by using $(Et_4N)[^{54}Fe(2,6\text{-dimethylphenolate})_4]$[14] as the starting material.

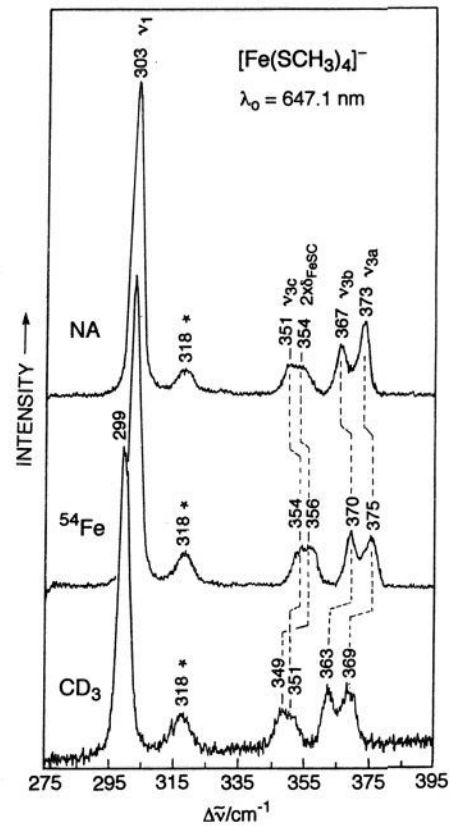

Figure 2. RR spectra of $(Et_4N)[Fe(SCH_3)_4]$ (top) and its ^{54}Fe (middle) and CD_3 (bottom) isotopomers at 77 K in KCl pellets obtained with 647.1-nm excitation (100 mW) and 3-cm^{-1} slit widths. The spectrometer was advanced in 0.2 cm^{-1}/s intervals. Asterisks mark bands associated with a photodecomposition product. NA = natural abundance.

The $(Et_4N)[Fe(S_2\text{-}o\text{-xyl})_2]$ complex was synthesized by the procedure described in ref 9 except that lithium ethoxide was substituted for sodium ethoxide. The *o*-xylene-α,α'-dithiol was freshly prepared and sublimed before use. The analog with deuterium substituted for the eight methylene hydrogen atoms was prepared by the same procedure, utilizing the ligand *o*-xylene-d_4-α,α'-dithiol, whose preparation was described previously.[7] The ^{34}S isotopomer was prepared with $(H^{34}S)_2$-*o*-xylyl, which was obtained from the reaction of α,α'-dibromo-*o*-xylene with (^{34}S)thiourea (93% enriched, ICON). ^{54}Fe substitution was carried out by using anhydrous $^{54}FeCl_3$, prepared via reaction of $^{54}Fe_2O_3$ (97% enriched, Oak Ridge National Laboratories) with thionyl chloride in a sealed tube.[15]

Infrared and Resonance Raman Spectra. Low-temperature (77 K) infrared spectra were obtained as described previously,[16] with a Digilab FT20C Fourier transform infrared spectrometer equipped with a N_2 purge sample chamber. Resonance Raman spectra were collected in a backscattering geometry from the surface of a frozen solution (pyridine) or a KCl pellet kept in a liquid-N_2 dewar.[17] All samples were stable under prolonged laser irradiation at 568.2 and 647.1 nm, but significant photodecomposition was observed when shorter wavelengths were used.

Excitation lines were provided by Spectra Physics 171 Kr^+ and 2025 Ar^+ ion lasers. The laser power at the sample was typically 100 mW. The scattered light was dispersed in a Spex 1401 double monochromator and detected by a cooled RCA 31034 photomultiplier tube with an ORTEC 9315 photon counting system, under the control of a MINCII (DEC) minicomputer. Polarization measurements were carried out on the solid samples (KCl pellet) by analyzing the 180° scattered light in front of the monochromator slit.[18] The Raman spectra shown in the figures are typically the sum of 5–8 scans with 0.2 or 0.5 cm^{-1}/s increments.

(10) (a) Han, S.; Czernuszewicz, R. S.; Spiro, T. G. *J. Am. Chem. Soc.* **1989**, *111*, 3496–3504. (b) Han, S.; Czernuszewicz, R. S.; Kimura, T.; Adams, M. W. W.; Spiro, T. G. *J. Am. Chem. Soc.* **1989**, *111*, 3505–3511.

(11) Kilpatrick, L. K.; Kennedy, M. C.; Beinert, H.; Diu, D.; Czernuszewicz, R. S.; Spiro, T. G. *J. Am. Chem. Soc.* **1994**, *116*, 4053–4061.

(12) Saito, H.; Imai, T.; Wakita, K.; Urushiyama, A.; Yagi, T. *Bull. Chem. Soc. Jpn.* **1990**, *64*, 829–836.

(13) (a) Koch, S. A.; Maelia, L. E.; Millar, M. *J. Am. Chem. Soc.* **1983**, *105*, 5944–5945. (b) Maelia, L. E.; Millar, M.; Koch, S. A. *Inorg. Chem.* **1992**, *31*, 4594–4600.

(14) Koch, S.; Millar, M. *J. Am. Chem. Soc.* **1982**, *104*, 5255–6267.

(15) North, H. B.; Hageman, A. M. *J. Am. Chem. Soc.* **1913**, *35*, 352–356.

(16) Czernuszewicz, R. S.; Macor, K. A.; Johnson, M. K.; Gewirth, A.; Spiro, T. G. *J. Am. Chem. Soc.* **1987**, *109*, 7178–7187.

(17) Czernuszewicz, R. S.; Johnson, M. K. *Appl. Spectrosc.* **1983**, *37*, 297–298.

(18) (a) Strommen, D. P.; Nakamoto, K. *Appl. Spectrosc.* **1983**, *37*, 436–439. (b) Strommen, D. P.; Bajdor, K.; Czernuszewicz, R. S.; Blinn, E. L.; Nakamoto, K. *Inorg. Chim. Acta* **1982**, *63*, 151–155.

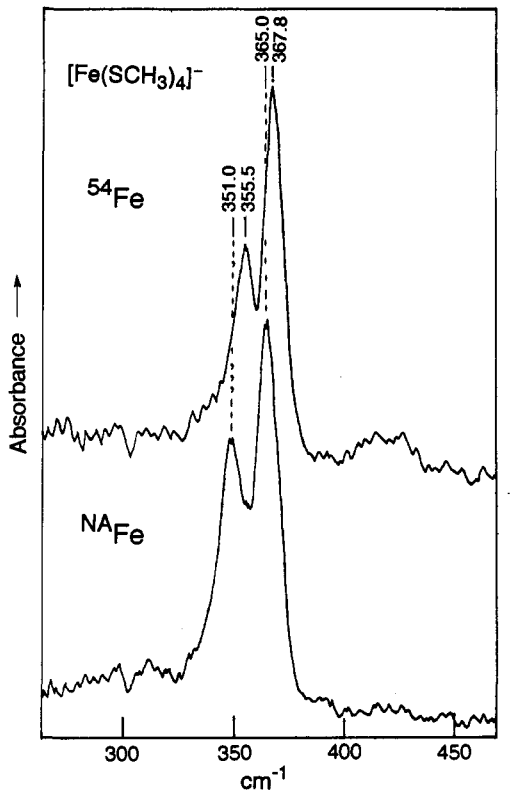

Figure 3. Low-temperature (77 K) infrared spectra of $(Et_4N)[Fe(SCH_3)_4]$ and its ^{54}Fe (top) isotopomer obtained with a Digilab FTS-20C FTIR spectrophotometer. The samples were Nujol mulls and were sealed between polyethylene plates.[16]

Normal Mode Analysis. Normal mode calculations were carried out using the GF matrix method and a Urey-Bradley force field.[19] Schachtschneider's programs were employed for constructing the G matrices and for solving the secular equations.[20]

Results

Using RR and IR spectroscopy, we have collected vibrational data on the analog complexes $[Fe(SMe)_4]^-$, $[Fe(SEt)_4]^-$, and $[Fe(S_2\text{-}o\text{-}xyl)_2]^-$ (structures shown in Figure 1) and on selected isotopomers, in the region of the Fe—S vibrations and the modes to which they are coupled. Spectra are presented in Figures 2 and 3 for $[Fe(SMe)_4]^-$, Figures 4 and 5 for $[Fe(SEt)_4]^-$, and Figures 6–8 for $[Fe(S_2\text{-}o\text{-}xyl)_2]^-$; spectra of oxidized Rd from *Desulfovibrio gigas* are reproduced from ref 8 in Figure 9. Assignments for these complexes, and for Rd, are given in Tables 1 and 2. These assignments were made with the aid of normal coordinate analysis (NCA) calculations, using the crystallographic structure parameters listed in Table 3 and the force constants given in Table 4. The force constants were taken from the literature and adjusted to give satisfactory frequencies and isotope shifts for all four molecules, with only slight differences among them (discussed below). All the constants have physically reasonable values. The Fe—S stretching constant was adjusted to reflect the slight differences in Fe—S bond lengths, via Badger's rule.[21]

In T_d symmetry, the four Fe—S stretches group themselves into a totally symmetric breathing mode, ν_1, and a triply degenerate asymmetric mode, ν_3. Symmetry lowering splits the degeneracy, and up to three ν_3 components can be detected, labeled ν_{3a}, ν_{3b}, and ν_{3c}, in order of decreasing frequency. In addition, other coordinates may give rise to vibrational bands in the same frequency region and may couple to the Fe—S stretches. These symmetry-lowering and coupling effects are considered systematically in the context of the mode assignments of the analog complexes and of Rd in the following sections.

1. $[Fe(SMe)_4]^-$. The methanethiolate complex is the simplest $[Fe(SR)_4]^-$ species, yet its RR spectrum, shown in Figure 2, is

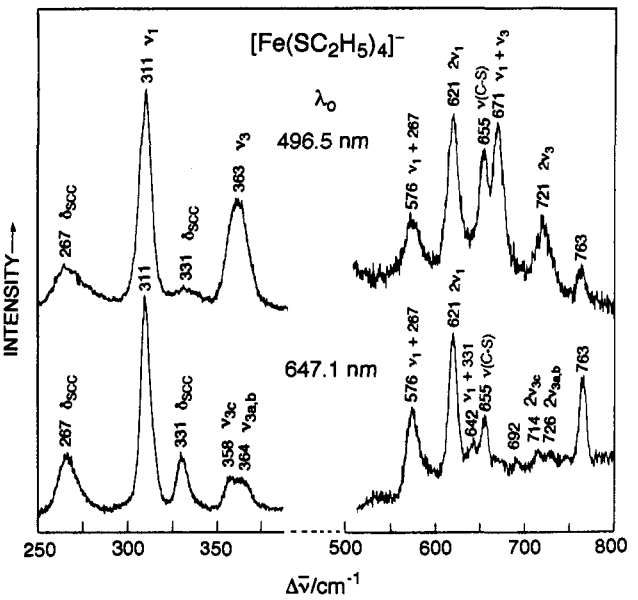

Figure 4. RR spectra of $(Pr_4N)[Fe(SC_2H_5)_4]$ at 77 K in KCl pellets obtained with 496.5-nm (top) and 647.1-nm (bottom) laser excitations (100 mW), 5-cm^{-1} slit widths, and 0.5 cm^{-1}/s intervals.

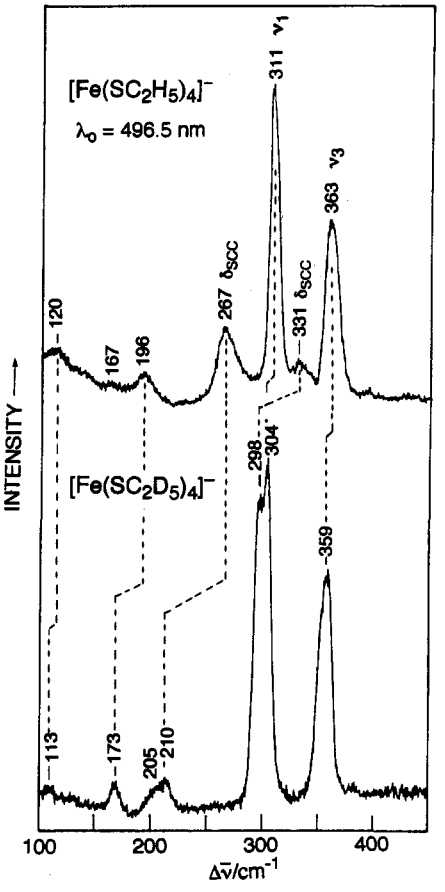

Figure 5. RR spectra of $(Pr_4N)[Fe(SC_2H_5)_4]$ and its d_{20} isotopomer at 77 K in KCl pellets obtained with 496.5-nm excitation (100 mW), 6-cm^{-1} slit widths, and 0.5 cm^{-1}/s intervals.

(19) Wilson, E. B.; Decius, J. C.; Cross, P. C. *Molecular Vibrations*; McGraw-Hill: New York, 1955.

(20) Schachtschneider, J. H. Shell Development Co., Technical Report No. 57–65 and 231–264, 1962.

(21) $k_0 = 1.86 \times 10^6 (r_e - d_{ij})^{-3}$ mdyn/Å, where r_e = equilibrium bond distance and $d_{ij} = 1.02$ for Fe—S bonds. (a) Badger, R. M. *J. Chem. Phys.* **1934**, *2*, 128–131. (b) Hershbach, D. R.; Laurie, V. W. *J. Chem. Phys.* **1961**, *35*, 458–462.

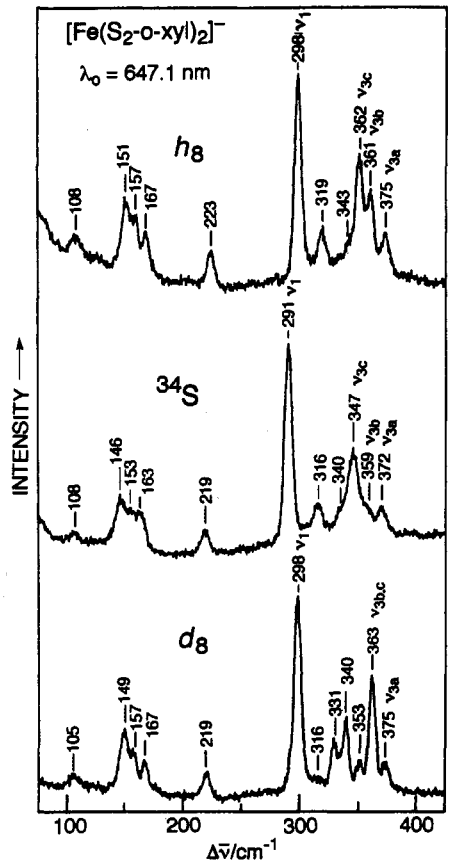

Figure 6. RR spectra of $(Et_4N)[Fe(S_2\text{-}o\text{-}xyl)_2]$ (top) and its ^{34}S (middle) and CD_2 (bottom) derivatives at 77 K in KCl pellets obtained with 647.1-nm laser excitation (100 mW), 5-cm^{-1} slit widths, and 0.5 cm^{-1}/s intervals.

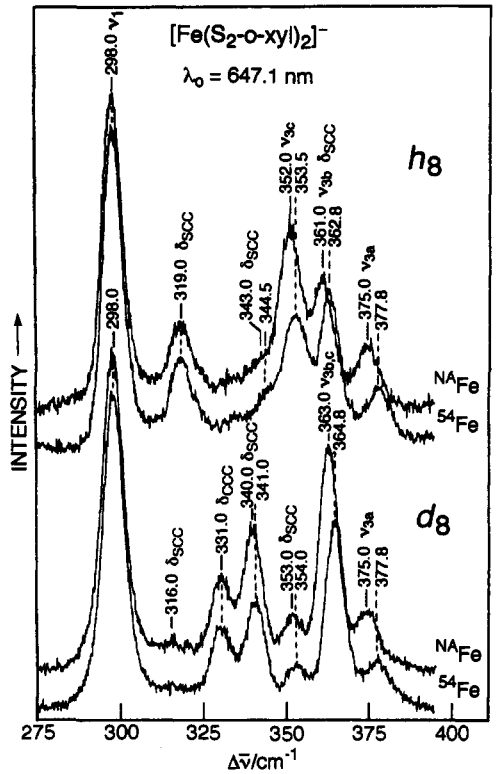

Figure 7. RR spectra of $(Et_4N)[Fe(S_2\text{-}o\text{-}xyl)_2]$ and its ^{54}Fe isotopomer with either hydrogen (top) or deuterium (bottom) labeled methylene groups at 77 K in KCl pellets obtained as in Figure 6, but with 0.2 cm^{-1}/s intervals.

far from simple. A strong band arising from ν_1 is seen at 303 cm^{-1}; it shifts 4 cm^{-1} to lower frequency upon ligand perdeuteration, reflecting the increase in effective mass, but shows no effect of ^{54}Fe substitution, since the Fe atom does not move in the breathing mode. Instead of a single ν_3 band, three ^{54}Fe-sensitive bands are seen, at 373, 367, and ca. 352 cm^{-1}; their 2–3-cm^{-1} ^{54}Fe upshifts agree well with expectation for the ν_3 mode and with the normal mode calculation of the three ν_3 components of $[Fe(SMe)_4]^-$ (Table 1).

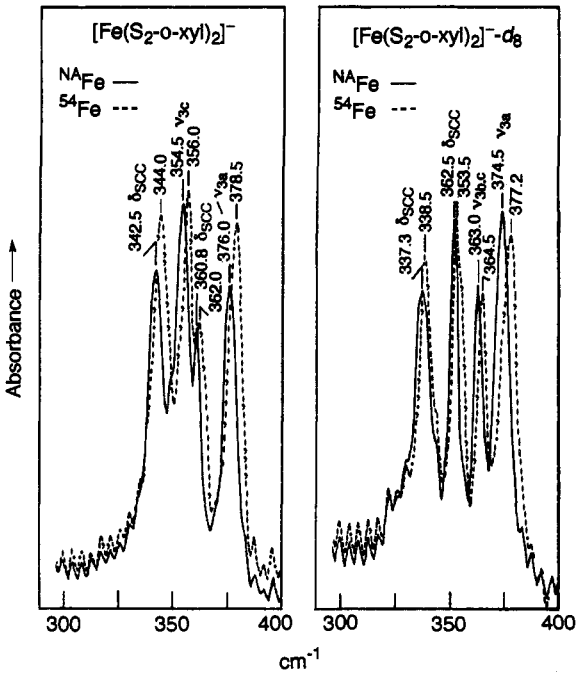

Figure 8. Low-temperature (77 K) infrared spectra of $(Et_4N)[Fe(S_2\text{-}o\text{-}xyl)_2]$ (solid line) and its ^{54}Fe isotopmer (broken line) with either hydrogen (top) or deuterium (bottom) labeled methylene groups obtained as in Figure 3.

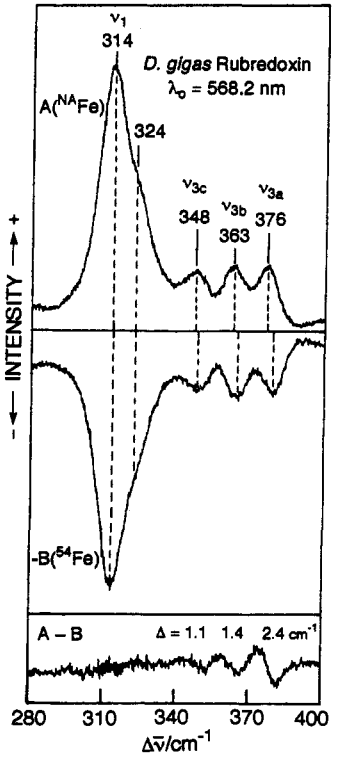

Figure 9. RR spectra of oxidized *D. gigas* rubredoxin (A), its ^{54}Fe reconstituted protein (–B), and corresponding difference spectrum (A – B) showing $^{54/56}Fe$ isotope shifts. Both spectra were obtained in a tuning fork difference Raman cell (liquid N_2)[25] with 568.2-nm excitation (200 mW), 4-cm^{-1} slit widths, and 0.2 cm^{-1}/s intervals (12 scans each), redrawn from ref 8.

Table 1. Observed and Calculated Frequencies and Isotope Shifts (cm^{-1}) for $[Fe(SMe)_4]^-$, $[Fe(SEt)_4]^-$, and Rubredoxin[a]

	$[Fe(SMe)_4]^-$							$[Fe(SEt)_4]^-$					rubredoxin[c]				
			$\Delta^{54}Fe$		Δd_{12}					Δd_{20}					$\Delta^{54}Fe$		
mode	obs	calc	obs	calc	obs	calc	PED (%)[b]	obs	calc	obs	calc	PED (%)	obs	calc	obs[c]	calc	PED (%)
							FeS					FeS, SCC, τ					FeS, SCC
ν_{3a}	373	370	2	3	4	1	84	364	364	4	5	80, 0, 0	376	377	2.5	2.3	72, 18
ν_{3b}	367	364	3	3.5	4	2	94		365			74, 0, 0	363	368	1.5	1.9	65, 22
ν_{3c}	352	351	3	3	0	1	96	358	361			88, 0, 0	348	352	1.1	3.2	92, 0
									339		31	0, 77, 0					
								331	333	33	30	0, 64, 0	324	324	0	0.6	28, 44
									334		31	0, 76, 0		316		0	0, 62
									332		32	0, 74, 0					
ν_1	303	302	0	0	4	4	88	311	310	7	10	68, 0, 18	314	315	0	0.5	38, 39
														273		1.2	20, 50
														244		0.7	36, 33
												τ, SFeS, FeSC					τ, SFeS, FeSC
								267	262	57	63	70, 0, 0	184	155			0, 35, 31
								240	250		61	70, 0, 0	174	151			0, 37, 30
									263		61	78, 0, 0		123			0, 50, 15
									259		66	66, 0, 0		119			0, 39, 14
							SFeS, FeSC										
		175		1		7	23, 68	196	152	23	14	0, 31, 48	150	107			15, 15, 39
		175		1		8	22, 71	167	144		12	0, 24, 52	130	103			46, 15, 15
		144		0		9	22, 68	120	121	7	7	0, 36, 46		100			0, 18, 47
		143		0		10	21, 67		121			0, 34, 44		98			19, 5, 47
		112		0		1	99, 0		100			0, 67, 20		85			24, 32, 17
		95		0		5	68, 27		87			0, 50, 40		72			24, 32, 17
		94		0		5	62, 32		82			0, 41, 44		68			28, 28, 17
		92		0		6	67, 31		81			0, 40, 48		53			33, 28, 11
		73		0		6	72, 25		64			0, 62, 30		46			42, 25, 6

[a] $\Delta^{54}Fe = \nu(^{54}Fe) - \nu(^{56}Fe)$; $\Delta d_{12} = \nu(SCH_3) - \nu(SCD_3)$; $\Delta d_{20} = \nu(SC_2H_5)_4 - \nu(SC_2D_5)_4$; τ = (HC—CH) torsion. [b] Percentage contribution to the potential energy distribution from the indicated coordinates. [c] Reference 8.

Table 2. Observed and Calculated Frequencies and Isotope Shifts (cm^{-1}) for $[Fe(S_2\text{-}o\text{-}xyl)_2]^-$

	$[Fe(S_2\text{-}o\text{-}xyl)_2]^-$							$[Fe(S_2\text{-}o\text{-}xyl)_2]^-\text{-}d_8$[a]				
mode	obs	calc	obs	calc	obs	calc	PED (%)[b]	obs	calc	obs	calc	PED (%)
							FeS, SCC, CCC					
	396	398		0		1	8, 0, 69					
		397		0		0	4, 0, 69					FeS, SCC, CCC
ν_{3a}	375	375	2.8	2	3	3	44, 28, 6	375	375	2.8	2	56, 16, 0
	361	366	1.2[c]	1		3	29, 42, 0					
ν_{3b}	361	360	1.8	3	2	5	80, 4, 0	363	366	1.8	2	62, 2, 8
ν_{3c}	352	352	1.5	2	5	4	60, 20, 0	363	363	1.8	2	62, 12, 4
	343	343	1.5[c]	1	3	4	56, 28, 0	353	356	1.0	0	0, 56, 10
								340	340	1.0	1	46, 34, 0
								337[c]	338	1.2[c]	1	24, 0, 36
								331	335	0	1	30, 4, 36
	319	325	0	0	3	3	0, 44, 24		319		0	0, 42, 26
	319	324	0	0	3	3	0, 44, 24		318		0	0, 42, 29
ν_1	298	297	0	0	7	4	88, 0, 0	298	295	0	0	86, 0, 0
	223	252		0	4	0	0, 0, 59	219	210		0	0, 0, 60
		251		0		0	0, 0, 59		209		0	0, 0, 60
							SFeS, FeSC					SFeS, FeSC
	167	148			4	2	36, 42		167	147		36, 40
	157	138			4	2	47, 40		157	135		53, 32
	151	123			5	2	68, 24		149	121		76, 12
	125	116				2	44, 54		113			46, 36
	108	105			0	1	10, 64		105	100		6, 68

[a] Methylene groups deuterated. [b] Potential energy distribution (as Table 1). [c] From IR; other values from RR.

The ν_{3c} band is further split into two components, at 354 and 351 cm^{-1}. This splitting is attributable to a Fermi resonance between ν_{3c} and the overtone of an Fe—S—C bending mode, δ_{FeSC}. There are four such modes in $[Fe(SMe)_4]^-$, which the normal mode calculation places between 140 and 175 cm^{-1} (Table 1). The highest of these is close to half the frequency of ν_{3c}, so a Fermi resonance with its overtone is expected. The NCA predicts a small 1-cm^{-1} shift for ν_{3c} upon ligand perdeuteration, but a 7-cm^{-1} shift for the 175-cm^{-1} δ_{FeSC} mode, accounting for the CD_3 sensitivity of the Fermi doublet. The Fermi resonance also accounts for the curious observation that in the IR spectrum (Figure 3) the ν_{3c} band seems to shift up 4.5 cm^{-1} upon ^{54}Fe substitution, more than is possible for a pure ν_3 mode. By comparison with the RR spectrum, it is apparent that the IR intensity is concentrated in the lower component of the Fermi doublet in the natural abundance sample, but in the higher component in the ^{54}Fe sample. Evidently the isotope substitution alters the eigenvectors of the Fermi components to produce this switch in the dipole strength.

The splitting of ν_3 into three well-separated components implies significant symmetry lowering from T_d. Two sources of symmetry lowering can be seen in the crystal structure[13b] of $[Fe(SMe)_4]^-$. (1) The S—Fe—S angles deviate from tetrahedral values; two of them are lowered to 107°, producing an elongated tetrahedron, while the remaining four are expanded to 114°. The distortion is presumably due to crystal packing forces, since the ethanethi-

Table 3. Averaged Fe—S Bond Distances (Å), S—Fe—S Angles (deg), and Dihedral Angles (deg) about the Fe—S and S—C Bonds for the Analog Complexes and Rubredoxin

	$Fe(SMe)_4]^-$ [a]	$[Fe(SEt)_4]^-$ [b]	$[Fe(S_2\text{-}o\text{-}xyl)_2]^-$ [c]	rubredoxin[d]
d(Fe—S)	2.264	2.269	2.268	2.29
$\angle$(S—Fe—S)$_4$[e]	114	109.5	110.6	111.8
$\angle$(S—Fe—S)$_2$	107	109.5	107	104.8
τ(SFe—SC)	54		60	66
τ(SFe—SC)		90	90	90, 180[f]

[a] Et_4N^+ salt.[13b] [b] Pr_4N^+ salt.[13a] [c] Et_4N^+ salt.[9] [d] Structural parameters taken from the X-ray crystal structure of the oxidized rubredoxin from *C. pasteurianum*.[2] [e] Subscripts indicate number of equivalent S—Fe—S angles. [f] Two of the FeS—CC dihedral angles are 90° and two are 180°.

Table 4. Force Constants[a] Used for Normal Mode Calculations on $[Fe(SMe)_4]^-$, $[Fe(SEt)_4]^-$, $[Fe(S_2\text{-}o\text{-}xyl)_2]^-$,[b] and Rubredoxin

K(FeS)[c]	1.34	τ(HC—CH)[e]	0.0216
K(SC)	3.05	F(S···S)	0.0335
K(CC)	4.80	F(Fe···C)	0.12
K(CH)	4.70	f(FeS/FeS)	0.07
H(SFeS)	0.35	f(SC/SCC)	0.35
H(FeSC)	0.25	f(CC/SCC)	0.35
H(SCC)	0.82	f(FeSC/SCH)[f]	0.22
H(HCH)	0.54		
H(SCH)	0.62		
H(CCH)[d]	0.62		

[a] K = stretching (mdyn/Å); H = bending (mdyn Å/rad²); F = nonbonded interaction (mdyn/Å); f = stretch–stretch valence interaction (mdyn/Å) and stretch–bend valence interaction (mdyn/rad). [b] Additional force constants for $[Fe(S_2\text{-}o\text{-}xyl)_2]^-$: H(CCC) = 1.10, for angles within the benzene ring, and 0.80 for the angle between the ring methylene bond and the adjacent ring bonds; F(S···C) = 0.06; f(SC/SCC) = 0.65; K(C=C) = 5.90. [c] Values were 1.35 for $Fe[(SMe)_4]^-$ and 1.27 for Rd. [d] Not applicable to $Fe[(SMe)_4]^-$. [e] Not applicable to $[Fe(SMe)_4]^-$ and $[Fe(S_2\text{-}o\text{-}xyl)_2]^-$. [f] f(FeSC/SCH) = 0.12 for $[Fe(SMe)_4]^-$.

olate complex has essentially tetrahedral bond angles (see below). (2) The S—C bonds are rotated out of the S—Fe—S planes, producing SFe—SC dihedral angles of 54°.

The nontetrahedral S—Fe—S angles cannot in themselves produce three ν_3 components, since the elongated tetrahedron has D_{2d} symmetry, and two components are therefore expected (E + B_2). Indeed, two components are calculated, at 369 and 354 cm^{-1} when the SFe—SC dihedrals were changed to 0°, to achieve D_{2d} symmetry. The latter value agrees with the observed ν_{3c} frequency, while the former falls between ν_{3a} and ν_{3b}. Thus, the $\nu_{3a/b}$ splitting is attributed to the out-of-plane S—C bonds, the S—Fe—S angular distortion accounting for ca. 15 cm^{-1} and the S—C bond rotation for ca. 6 cm^{-1} of the ~21-cm^{-1} ν_3 splitting. To confirm this, as well as to obtain evidence that the elongated tetrahedron arises from crystal packing forces, we have recorded the spectrum (not shown) of $[Fe(SMe)_4]^-$ in solution (frozen pyridine) and observed only a broad band in the ν_3 region with discernible components at 357 and 364 cm^{-1}.

It is interesting that in the IR spectrum (Figure 3) ν_{3b} and ν_{3c} are seen, but ν_{3a} is not. We attribute this lack of dipole strength for ν_{3a} to the C_2 symmetry of the molecule and the splitting of the E component of ν_3 into A and B symmetry species. The A component is identified with ν_{3a}.

In summary, the complexity of the ν_3 region of the solid-state vibrational spectrum of $[Fe(SMe)_4]^-$ is due to symmetry lowering from nontetrahedral S—Fe—S angles and from the S—C bonds being oriented out of the S—Fe—S planes. There is an additional Fermi resonance between the lowest ν_3 component and an Fe—S—C bending overtone.

2. $[Fe(SEt)_4]^-$. When the RR spectrum (Figure 4) of $[Fe(SEt)_4]^-$ is examined, ν_3 is collapsed to a single band, ~363 cm^{-1}, as expected from the essentially tetrahedral values for all of the S—Fe—S angles.[13a] The band is broad, however, and when the laser wavelength is tuned to 647.1 nm, away from resonance with the S → Fe CT transitions, a second component can be seen, at 358 cm^{-1}. This frequency is confirmed by examining the overtone region (Figure 4), where distinct bands at 715 and 726 cm^{-1} are seen, double the frequencies of the 364- and 358-cm^{-1} ν_3 components. The 364-cm^{-1} component is more strongly enhanced as the laser wavelength approaches resonance. This 6-cm^{-1} splitting of ν_3 is reproduced in the NCA calculation (Table 1) and is attributable to the same symmetry lowering via out-of-plane S—C orientation that produced the 6-cm^{-1} ν_{3a}/ν_{3b} splitting in $[Fe(SMe)_4]^-$.

Deuteration of the four ethyl groups (d_{20}) shifts both ν_3 and ν_1 by several cm^{-1} (Figure 5), as it does for $[Fe(SMe)_4]^-$. In addition, this experiment also identifies one of the S—C—C bending modes (δ_{SCC}) with the RR band at 331 cm^{-1}, shifting down 33 cm^{-1} upon perdeuteration. One of the δ_{SCC} modes is calculated at this frequency, with the observed perdeuteration shift, and the others are calculated nearby. The 331-cm^{-1} band is only weakly enhanced, as expected for a ligand bending mode (it gains relative intensity off resonance at 647.1 nm, Figure 4), but in the d_{20} spectrum (Figure 5) it borrows intensity from ν_1, with which it is accidentally nearly coincident. There is little kinematic interaction among the δ_{SCC} and ν(FeS) coordinates, however, because the coordinates are essentially orthogonal, since the FeS—CC dihedral angles are 90°. This lack of interaction is evidenced by the fact that the average frequency of the ν_3 components is the same for $[Fe(SEt)_4]^-$ as it is for $[Fe(SMe)_4]^-$, which has no δ_{SCC} coordinates.

Strikingly, however, ν_1 is *not* at the same frequency for the two complexes; it is 8 cm^{-1} higher for $[Fe(SEt)_4]^-$. This elevation is due to kinematic interaction with another coordinate, which is missing in $[Fe(SMe)_4]^-$, namely, the HC—CH torsional coordinate. When the force constant for this coordinate is set to 0, ν_1 is calculated to decrease by 12 cm^{-1}, which is in agreement with the ν_1 frequency of $[Fe(SMe)_4]^-$. A torsional mode is identified at 267 cm^{-1} in the RR spectrum of $[Fe(SEt)_4]^-$ (Figure 5) via its 57-cm^{-1} d_{20} downshift; it is moderately strong, reflecting the mixing with ν_1. This mode is calculated at 262 cm^{-1}, with a 63-cm^{-1} expected isotope shift, and another torsional mode is calculated at 250 cm^{-1}. No band is seen at this position, but the d_{20} spectrum has a 205-cm^{-1} shoulder on the 210-cm^{-1} band. With 647.1-nm excitation (Figure 4), a band is seen at 240 cm^{-1}, which may be the second torsional mode.

At lower frequencies, additional isotope-sensitive bands are seen, at 196, 167, and 120 cm^{-1}. These correspond to modes calculated to arise from Fe—S—C and S—Fe—S bending modes. In the 550–750-cm^{-1} region, overtone and combination bands involving ν_1 and ν_2 are seen, and a band at 655 cm^{-1} is assigned to S—C stretch.[22]

3. $[Fe(S_2\text{-}o\text{-}xyl)_2]^-$. The $[Fe(S_2\text{-}o\text{-}xyl)_2]^-$ complex, the first successful analog of the rubredoxin active site,[9] gives a surprisingly complex set of spectra (Figures 6–8). At first glance the RR spectrum (both the solid state and solution) resembles that of solid $[Fe(SMe)_4]^-$, with a ν_1 band at 298 cm^{-1} and three widely separated ν_3 components, at 352, 361, and 375 cm^{-1}. With respect to ν_1 the resemblance to $[Fe(SMe)_4]^-$ rather than $[Fe(SEt)_4]^-$ is gratifying, because the mechanism for ν_1 elevation in $[Fe(SEt)_4]^-$, namely, interaction with HC—CH torsional modes, is not applicable to $[Fe(S_2\text{-}o\text{-}xyl)_2]^-$. The C atom connected to the SCH_2 unit is part of the benzene ring (Figure 1), so there is no HC—CH coordinate. On the other hand, $[Fe(S_2\text{-}o\text{-}xyl)_2]^-$ resembles $[Fe(SEt)_4]^-$ in having an extra band at 319 cm^{-1}, which may arise from S—C—C bending.

The wide splitting of ν_3 is unexpected, however, because the inequivalence of the S—Fe—S bond angles is only 3.6° in $[Fe(S_2\text{-}o\text{-}xyl)_2]^-$, compared to 7° in $[Fe(SMe)_4]^-$. Moreover, when the IR spectrum is examined (Figure 8), four bands are seen in the ν_3 region, instead of three. Because of this complexity, we prepared several isotopomers in order to clarify the mode

(22) Smith, D.; Devlin, J. P.; Scott, D. W. *J. Mol. Spectrosc.* **1968**, *25*, 174–184.

assignments: ^{34}S, ^{54}Fe, and d_8 (deuteration of the four methylene groups) and the doubly labeled species, d_8 and ^{54}Fe. Interpretation of the isotopomer spectra were guided by the normal mode calculation (Table 2), which revealed that, while two of the S—C—C bending modes are close to the observed 319-cm^{-1} band, the other two are elevated in frequency and interact strongly with the Fe–S stretching vibrations. This frequency elevation apparently results from kinematic constraints in the S—C—C—C—C—S chelate rings. As a consequence, there are actually five ^{54}Fe-sensitive modes in the ν_3 region. Instead of the 3-cm^{-1} shifts expected for purely ν(Fe–S) components of ν_3, the calculated shifts are smaller, and variable, depending on the extent of coordinate mixing. The total shift of the five modes, however, is 9 cm^{-1}, the same as the total for the three ν_3 components of $[Fe(SMe)_4]^-$ (Table 1). These calculated shifts permit us to assign the RR and IR spectra with confidence, even though not all the modes are detected. The three modes with the highest ν(Fe—S) contributions to the potential energy distribution, and the largest ^{54}Fe shifts, are assigned to ν_{3a}, ν_{3b}, and ν_{3c} (376, 361, and 352 cm^{-1}). ν_{3b} overlaps with the highest of the two δ_{SCC} modes, producing a single band at 361 cm^{-1} in both the RR and IR spectra. The isotope shifts are between the calculated shifts for ν_{3b} and δ_{SCC}, 3 and 1 cm^{-1}. The IR band shift, 1.2 cm^{-1}, indicates that δ_{SCC} actually makes the dominant contribution to the band. Apparently, ν_{3b} is weak in the IR, suggesting cancellation of the dipole via symmetric phasing of the Fe—S stretches, as in the case of the ν_{3a} component in the $[Fe(SMe)_4]^-$ spectrum. S—C—C bending contributes less to the RR intensity, as can also be seen for the second δ_{SCC} mode, at 343 cm^{-1}, which is strong in the IR, but gives only a weak shoulder in the RR spectrum.

Deuteration of the methylene groups is calculated to unmix the five modes to a significant extent. The three highest modes, 375, 366, and 363 cm^{-1}, are now calculated to be predominantly Fe—S stretching, with 2-cm^{-1} ^{54}Fe shifts, while the lower two modes, 356 and 340 cm^{-1}, have greater S—C—C bending character and have 0–1.0-cm^{-1} ^{54}Fe shifts. The observed spectra are consistent with these expectations. The near-coincidence of ν_{3b} and ν_{3c} account for the high intensity of the 363-cm^{-1} band. Likewise, the two near-coincident δ_{SCC} modes give a single vibrational band. Interestingly, this band is prominent in the d_8 RR spectrum, although the δ_{SCC} bands are weak in the h_8 spectrum.

Another curious feature of the d_8 RR spectrum is the disappearance of the 319-cm^{-1} band and the appearance of a new band at 331 cm^{-1}. The calculation (Table 2) indicates that these two bands do not arise from the same mode. The lower frequency pair of S—C—C bends, to which the 319-cm^{-1} h_8 band is assigned, are calculated to be present in the d_8 molecule, shifting down by only 6 cm^{-1}. A new, ^{54}Fe-insensitive band is calculated at 335 cm^{-1}, whose potential energy distribution shows it to be mainly a C—C—C bend, δ_{CCC}, mixed with Fe—S stretching. The closest correspondence in the h_8 calculation is a δ_{CCC} mode at 398 cm^{-1}. A band is seen at 396 cm^{-1} in the IR spectra of $[Fe(S_2\text{-}o\text{-}xyl)_2]^-$ that was reported to shift to 352 cm^{-1} when $[Fe(S_2\text{-}o\text{-}xyl)_2]^-$ was perdeuterated.[7] Similarly, in the IR spectrum of the free ligand, o-xylylene-α,α'-dithiol (shown in Figure 4 of ref 7), there is a band at 390 cm^{-1} which is replaced in the d_8 isotopomer with a band at 350 cm^{-1}. On the basis of these findings, we infer that the methylene deuteration shifts a δ_{CCC} mode substantially and induces RR intensity via mixing with the Fe—S stretching coordinates. The reason for the loss of RR enhancement for the ~320-cm^{-1} S—C—C bending modes is unclear, however, since in neither isotopomer is a significant ν(Fe—S) contribution calculated. Several ^{34}S- and/or d_8-sensitive bands are seen below 250 cm^{-1} (Figure 6) and arise from various bending coordinates (Table 2).

4. Rubredoxin. The RR spectrum of ^{54}Fe-labeled *D. gigas* Rd is reproduced in Figure 9 from our earlier study.[8] The strong ν_1 band, centered at 314 cm^{-1}, has a prominent shoulder at 324 cm^{-1}, which is ^{54}Fe-insensitive, and the three bands in the ν_3 region, 376, 363, and 348 cm^{-1}, have smaller ^{54}Fe shifts than the 3 cm^{-1} expected for pure ν_3 components. Lower frequency bands, attributed to Fe—S—C and S—Fe—S bending, have been observed at 184, 174, 150, and 130 cm^{-1}, and their excitation profiles have been analyzed in terms of the D_{2d} optical symmetry of the chromophore.[8]

As in the case of $[Fe(SEt)_4]^-$, the ν_1 frequency of oxidized Rd is elevated, relative to $[Fe(SMe)_4]^-$ and $[Fe(S_2\text{-}o\text{-}xyl)_2]^-$, but the mechanism is different. The mixing of ν_1 with the HC—CH torsional modes is much less for Rd than for $[Fe(SEt)_4]^-$, because the cysteine side chain does not have a methyl group attached to the SCH_2 unit. In the normal mode calculation shown in Table 1, we modeled the Rd active site with ethanethiolate ligands, in which a single methyl H atom was replaced by a C atom. This modification was sufficient to eliminate the group of four HC—CH torsional modes calculated at 250–265 cm^{-1} for $[Fe(SEt)_4]^-$, even though the HC—CH force constant was unaltered. These modes are specifically methyl torsions. In the Rd model calculation, the HC—CH torsional coordinates contribute mainly to modes near 100 cm^{-1}. The cysteine side chains themselves have only a single H atom on the C_α atom attached to SCH_2.

The mechanism for ν_1 elevation in Rd is interaction of Fe—S stretching with the S—C—C bending modes. Unlike the analog complexes, all of which have only 90° FeS—CC dihedral angles, Rd has two 90° and two 180° dihedrals.[2] Two of the δ_{SCC} modes therefore mix strongly with ν_1; its potential energy distribution shows similar contributions, 38% from Fe—S stretching and 29% from S—C—C bending. Two of the δ_{SCC} modes are calculated at frequencies *below* ν_1, 273 and 244 cm^{-1}, and two are calculated above, 316 and 324 cm^{-1}. This last mode has significant ν(Fe—S) character, 28%, and is assigned to the 324-cm^{-1} shoulder on ν_1; the calculated 0.6-cm^{-1} ^{54}Fe shift would be too small to be detected for an unresolved band. The 244-cm^{-1} mode also has a large Fe—S stretching contribution, 36%; it has not been detected, but would have been hidden by the coincident ice band in the frozen protein solution spectra. The interaction with δ_{SCC} elevates the calculated ν_1 mode substantially *above* 314 cm^{-1}, and in order to bring it back down to the observed frequency, we were forced to lower the Fe—S stretching force constant to 1.27 mdyn/Å, from the 1.34–1.35 mdyn/Å value used for the analog complexes.

Calculated frequencies for the three ν_3 components are in reasonable agreement with the experimental values. The spread of frequencies, similar to that seen for $[Fe(SMe)_4]^-$, is likewise attributable to an elongation of the FeS_4 tetrahedron, with similarly inequivalent (7° difference) S—Fe—S angles (Table 1). There is also significant mixing with the S—C—C bending modes, resulting in diminished ^{54}Fe shifts. These are in good agreement with experiment for ν_{3a} and ν_{3b}, but for ν_{3c}, the calculation shows no S—C—C mixing and a ^{54}Fe shift, 3.2 cm^{-1}, that is much larger than the 1.1-cm^{-1} observed shift. Evidently, the calculation does not model interactions properly for this mode.

Discussion

The isotope-selective RR and IR data on the three analog complexes help to clarify the molecular interactions that influence the RR spectra of oxidized Rd. The fact that we have been able to account satisfactorily for almost all the frequencies and isotope shifts of all four molecules with a self-consistent force field implies that these interactions are, in the main, well understood. We consider these interactions in turn.

1. Out-of-Plane S—C Bonds. The spectra of $[Fe(SEt)_4]^-$ permit us to assess the effect of the S—C bonds being rotated out of the S—Fe—S planes. This is a structural feature common to all three analog complexes, and to Rd. Even in the case of $[Fe(SMe)_4]^-$, for which there are no additional heavy atoms

constraining the geometry, the S—C bonds are not in the S—Fe—S planes.

In the case of $[Fe(SEt)_4]^-$, the FeS_4 core is an essentially perfect tetrahedron, and the S—C orientation is the structural element that lowers the symmetry from T_d. The effect is to split the triply degenerate ν_3 band into two resolvable components, with a 6-cm^{-1} separation; a 4-cm^{-1} separation is predicted by our calculation, which indicates the modes to be ca. 80% Fe—S stretching in character. The same 6-cm^{-1} separation is seen (the calculation predicts 6 cm^{-1}) for the ν_{3a} and ν_{3b} bands of $[Fe(SMe)_4]^-$, which would be degenerate if the S—C bonds were in the S—Fe—S planes. Thus, the symmetry-lowering effect is quite modest and might be missed in spectra of low resolution. Nevertheless, the S—C orientation might have a significant effect on the Fe—S force constant itself. In $[Fe(SMe)_4]^-$, the SFe—SC dihedral angles are 54°, quite close to the 60° angles calculated by Ueyama *et al.*[23] to maximize π-bonding interactions between the Fe d orbitals and the S lone pair orbitals. Thus, the non-coplanar S—C orientation may have an electronic origin. If the SFe—SC angles were forced into non-60° angles, the Fe—S bonds would be expected to weaken.

2. FeS_4 Distortion. The FeS_4 tetrahedron is elongated in crystalline $[Fe(SMe)_4]^-$, with a 7° difference between the two contracted and four expanded S—Fe—S angles. A 16-cm^{-1} splitting is calculated for this distortion (separation between ν_{3c} and the mean of ν_a and ν_{3b}), in excellent agreement with the 18-cm^{-1} observed splitting (Table 1). Thus, the S—Fe—S angle variation has a greater symmetry-lowering effect than the S—C orientation. Oxidized Rd also shows elongation of the FeS_4 tetrahedron, with the same 7° difference among the S—Fe—S angles. Therefore, a similar ν_3 splitting is expected and accounts for about half of the total spread, 28 cm^{-1}, among the observed ν_3 components; the rest is attributable mainly to interactions with S—C—C bending.

3. Methyl Torsions in $[Fe(SEt)_4]^-$. While the average frequency of the ν_3 components is essentially the same for $[Fe(SEt)_4]^-$ as for $[Fe(SMe)_4]^-$, the ν_1 frequency is 8 cm^{-1} higher. This elevation is shown by the calculation to result from a specific interaction with methyl torsional modes at about 260 cm^{-1}. $[Fe(SEt)_4]^-$ is the only complex with methyl groups next to the SCH_2. Our model calculation on Rd shows that replacement of just one of the methyl H atoms with a heavy atom is sufficient to eliminate this interaction.

4. Chelate Ring Constraints in $[Fe(S_2\text{-}o\text{-}xyl)_2]^-$. In $[Fe(SEt)_4]^-$, the S—C—C bending coordinates give rise to a set of four modes at about 330 cm^{-1}. Because of the 90° FeS—CC dihedral angles, these coordinates are essentially orthogonal to Fe—S stretching and interact very little with the ν(Fe—S) modes. The interaction is just enough to produce weak enhancement of a band at 331 cm^{-1} in the d_8 isotopomer. In $[Fe(S_2\text{-}o\text{-}xyl)_2]^-$, the FeS—CC dihedral angles are also 90°, but the second C atoms are part of the benzene rings, and this constraint produces heavy mixing of two of the S—C—C bending modes with the asymmetric Fe—S stretches. Consequently, there are no fewer than five ^{54}Fe-sensitive modes in the ν_3 region, and a complex spectral change is observed upon methylene deuteration.

5. Planar Fe—S—C—C Units in Rd and the Fe—S Bond Strength. Interaction between Fe—S stretching and S—C—C bending is also an important aspect of the Rd vibrational spectrum, but in this case the interaction results from 180° FeS—CC dihedral angles for two of the cysteine ligands. The S—C—C bending modes are split into two pairs, one near 260 cm^{-1} and the other near 320 cm^{-1}. The ν_1 frequency is strongly elevated by the interaction. Indeed, the calculation shows that the only reason that the frequency discrepancy with respect to the $[Fe(SMe)_4]^-$ analog is not greater than the observed 11 cm^{-1} is that the Fe—S stretching force constant is lowered in the protein. The lower force constant implies weaker Fe—S bonds. Badger's rule predicts a lengthening of the distance of 0.02 Å, on the basis of the force constant reduction from 1.34 to 1.27 mdyn/Å. The average Fe—S distance reported for Rd is in fact 0.02 Å longer than in the analogs, although this difference is below the uncertainty of the protein crystallography data. The weakening of the Fe—S bonds in the protein is attributable to the H-bonding revealed by the crystal structures[2] between protein donor groups and the cysteinate S atoms.[24] The H-bonds reduce the negative charge on the S atoms and reduce their donor strength.

The δ_{SCC}/ν(Fe—S) interactions also produces some mixing with the ν_3 components, lowering the ^{54}Fe shifts from the values expected for pure ν(Fe—S) vibrations. The shift diminution for ν_{3c} is not reproduced by the calculation, however, indicating that further refinement of the model is needed.

6. Mixing with Other Protein Modes. The unaccounted shift diminution for ν_{3c} may reflect mixing of protein modes beyond those encompassed by our modified $[Fe(SEt)_4]^-$ model for Rd. There are many protein modes in the 400-cm^{-1} region, where heavy atom (C, N, O) deformations are expected. Saito *et al.*[12] have investigated this matter by calculating all the modes of Rd, excluding only the hydrogenic modes. The calculation included all 390 non-hydrogen atoms in the 52 residues of *Desulfovibrio vulgaris* Rd. Similar calculations were carried out for Rd from *D. gigas*, with 399 atoms, and from *Clostridium pasteurianum*, with 423 atoms. Of the 1167 normal modes in the *D. vulgaris* Rd calculation, 146 fell in the 250–450-cm^{-1} region, of which 23 had non-negligible contributions from Fe—S stretching to their eigenvectors. The displacements of the four Fe—S bonds were substantially in-phase for the seven modes below 330 cm^{-1} and substantially out-of-phase for the 16 modes above this frequency. Particularly large displacements were found for the in-phase modes at 302 cm^{-1} and for the out-of-phase modes at 357, 388, 413, and 417 cm^{-1}. These frequencies are not far from the observed ν_1 and ν_3 bands. Saito *et al.*[12] emphasize, however, that, even for those modes having the largest ν(Fe—S) contributions, most of the potential energy is contributed by numerous angle-bending coordinates, spread widely over the protein. Some 15 residues were found to contribute significantly to these modes.

It is surprising that vibrational interactions should spread so widely through the polypeptide chain, and the calculation is difficult to evaluate because of its complexity. The force field was necessarily somewhat simplified, and there were no tests to evaluate its reliability in describing mode mixing, e.g. via isotope shift comparisons. Nevertheless, it is probably the case that our small molecule modeling approach neglects some significant interactions and that the protein environment should be taken into account in a more comprehensive treatment. The value of the analog-based analysis is in showing how vibrational interactions can propagate out from the FeS_4 center and influence the ν(Fe—S) modes. The fact that the same force field reproduces the frequencies and most of the isotope shifts for Rd and its different analogs lends confidence that the main features of the RR spectra are accounted for.

Acknowledgment. This work was supported by Robert A. Welch Foundation Grant E-1184 (to R.S.C.) and by NIH Grant GM 13498 (to T.G.S.).

(23) Ueyama, N.; Sugawara, T.; Tatsumi, K.; Nakamura, A. *Inorg. Chem.* **1987**, *26*, 1978–1981.

(24) From a 0.07–0.08 mdyn/Å smaller Fe—S stretching force constant in rubredoxin, the ν_1 frequency for an isolated FeS_4 tetrahedron is expected to be lowered by ~7–8 cm^{-1} as the result of hydrogen bonding.

(25) Eng, J. E.; Czernuszewicz, R. S.; Spiro, T. G. *J. Raman Spectrosc.* **1985**, *16*, 432–437.